International Journal of Heat and Mass Transfer 54 (2011) 5359–5367

Contents lists available at SciVerse ScienceDirect

International Journal of Heat and Mass Transfer

journal homepage: www.elsevier.com/locate/ijhmt

Critical heat flux of pool boiling on Si nanowire array-coated surfaces

Ming-Chang Lu [a,*], Renkun Chen [b], Vinod Srinivasan [c], Van P. Carey [c], Arun Majumdar [c,1]

[a] Department of Mechanical Engineering, National Chiao Tung University, Hsinchu 30010, Taiwan
[b] Department of Mechanical and Aerospace Engineering, University of California at San Diego, CA 92093, USA
[c] Department of Mechanical Engineering, University of California at Berkeley, CA 94720, USA

ARTICLE INFO

Article history:
Received 17 November 2010
Received in revised form 27 July 2011
Accepted 27 July 2011
Available online 23 August 2011

Keywords:
Pool boiling
Critical heat flux
Nanowires
Hydrodynamics

ABSTRACT

Pool boiling of saturated water on plain Si surfaces and surfaces covered with a dense array of Si nanowires (SiNWs) has been studied. Measured CHF and heat transfer coefficient (HTC) values of about 223 ± 5.61 W/cm^2 and 9 ± 1.60 W/cm^2 K, respectively, on the nanowire array-coated surface are among the highest reported in boiling heat transfer. Meanwhile, the CHFs on both nanowire-coated and Plain Si surfaces show a similar heater size dependence – the CHF increases as heater size decreases. The measured CHFs on both types of surfaces are approximately following the prediction of the hydrodynamic theory assuming the Helmholtz wavelength equal to the corresponded heater length. It suggests that the CHFs on both types of surfaces might be limited by pool hydrodynamics.

1. Introduction

With the increasingly growing concerns on climate change, the study of energy conversion, storage and transport has become a critical issue. More than 90% of the world's total power is generated by heat engines and 40% of the heat engines are based on the Rankine cycle. In such heat engines, boiling heat transfer plays an important role in several thermal devices such as boilers, heat exchangers, and condensers etc. One of the most important parameters of boiling heat transfer is the critical heat flux (CHF), which determines the maximum power density that could be handled by a boiling heat transfer device. Reaching CHF in a thermohydraulic system can often lead to catastrophic failures due to large temperature jumps, such as those found in nuclear meltdown. Therefore, enhancing the CHF can have a significant impact on many energy conversion and utilization systems. However, the exact mechanism leading to CHF in boiling heat transfer remains elusive so far, because of the highly complex phenomena in boiling. In general, the mechanisms of CHF can be classified into two categories: (1) far-field and (2) near field.

1.1. Far-field mechanisms

The most well-known CHF models are based on the hydrodynamic instability theory, first proposed by Zuber [1] and later modified by Lienhard and Dhir [2], which asserts that the occurrence of CHF is because of pool hydrodynamics. As the applied heat flux rises, the velocity of vapor columns increases, resulting in an increase of velocity shear between up-flowing vapor and down-flowing liquid. Eventually, the vapor columns become unstable, causing a large retarding force on down-flowing liquid and preventing liquid from returning to the heater surface. A vapor blanket is then formed on the heater surface, which manifests itself as the CHF. The model of CHF based on the hydrodynamics can be expressed as:

$$q_{CHF} = u_c \rho_v h_{fg} (A_v/A_s), \tag{1a}$$

$$u_c = \left(\frac{2\pi\sigma}{\rho_v \lambda_H}\right)^{1/2}, \tag{1b}$$

where u_c, ρ_v, h_{fg} and A_v/A_s in Eq. (1a) represent critical vapor velocity, vapor density, latent heat and an area ratio of vapor column and heater surface, respectively, and σ and λ_H in Eq. (1b) are the surface tension of liquid and the critical Helmholtz wavelength on vapor columns, respectively. The critical velocity in Eq. (1b) is obtained from a linearized instability analysis at an interface between two fluids with relative velocities [3,4]. This type of instability is referred to the Helmholtz instability [3,4], in which the velocity shear between two fluids disrupts the interface while surface tension of liquid tends to stabilize it. Zuber assumed that the Helmholtz wavelength (λ_H) should be equal to the perimeter of the vapor column ($\lambda_H = 2\pi R$), a condition of Plateau–Rayleigh instability of a liquid jet [5]. Meanwhile, in the transition boiling regime, an unstable vapor film forms underneath a liquid pool on the heater surface, a condition depicted by the Taylor instability [3,4,6]. By approaching

* Corresponding author.
E-mail address: mclu@mail.nctu.edu.tw (M.-C. Lu).
[1] Present address: Advanced Research Projects Agency-Energy, Department of Energy, Washington DC 20585, USA

0017-9310/$ - see front matter © 2011 Elsevier Ltd. All rights reserved.
doi:10.1016/j.ijheatmasstransfer.2011.08.007

Nomenclature

A_c	cross-sectional area
A_v	area covered by vapor
A_s	heater area
d	distance away from the heater edge (equals to 2 mm)
g	gravity
h_{fg}	latent heat of vaporization
K	proportional constant
k	thermal conductivity
L'	non-dimensional heater length
L	heater length
L_c	capillary length
l	liquid flowing distance
$\dot{m}_l$	liquid mass flow rate
q_{CHF}	critical heat flux
$q_{CHF,Z}$	critical heat flux predicted by Zuber
q_s	heat spread by conduction through substrate
R	radius of vapor column
r_c	critical radius of curvature
T_{edge}	temperature at the edge of the heater
T_{ref}	temperature at the point 2 mm away from the heater
u_c	critical velocity

Greek

θ	contact angle
κ	permeability
λ_C	critical Taylor wavelength
λ_D	most dangerous Taylor wavelength
λ_H	Helmholtz wavelength
μ	dynamic viscosity
ρ	density
ρ_l	liquid density
ρ_v	vapor density
σ	surface tension
Ω	angle relative to horizontal

Subscript

CHF	Critical heat flux
CHF,Z	Critical heat flux proposed by Zuber's model
l	liquid
v	vapor

the CHF point from the transition boiling regime, he postulated that the radius of vapor columns (R) and the separation of vapor columns equal to $\lambda_C/4$ and λ_C, respectively, where λ_C $(=2\pi[\sigma/g(\rho_l-\rho_v)]^{-1/2})$ is the critical wavelength of Taylor instability [3,6]. The area ratio of vapor columns and heater surface is then obtained as $\pi/16$, accordingly. The Helmholtz wavelength is derived as $\lambda_H = \pi\lambda_C/2$. Zuber further approximated the numerical term of $3/\sqrt{2\pi}$ as one to obtain the model of CHF expressed as:

$$q_{CHF} = 0.131\sqrt{\rho_v}h_{fg}[\sigma g(\rho_l-\rho_v)]^{1/4}, \tag{2}$$

where ρ_l is the liquid density. Lienhard and Dhir [2] claimed that the Helmholtz wavelength (λ_H) should be equal to the most dangerous Taylor instability wavelength λ_D ($\lambda_D = \sqrt{3}\ \lambda_c$ [3,6]) since this mode of disturbance will be the fastest growing mode once it appears in the system. This results in a different proportionality constant shown as:

$$q_{CHF} = 0.149\sqrt{\rho_v}h_{fg}[\sigma g(\rho_l-\rho_v)]^{1/4}. \tag{3}$$

It is worth noting that both Eqs. (2) and (3) have the same functional form as the model proposed by Kutateladze [7] based on a dimensional analysis:

$$q_{CHF} = K\sqrt{\rho_v}h_{fg}[\sigma g(\rho_l-\rho_v)]^{1/4}, \tag{4}$$

where K is found to be 0.16 from the experimental data.For the past few decades, although the predictions of CHF values based on the hydrodynamic instability theories agree with some of the experimental results [8], they cannot explain the dependence of CHFs on surface/material properties such as surface wettability [9–16], and spreading ability [17], surface capillarity [18,19], nucleation site density [20], thermal fin effect [21–23], etc.

1.2. Near-field mechanisms

Besides the hydrodynamic instability mechanism, which deals with the flow dynamics far away from the heater surface, there are other proposed CHF mechanisms which primarily consider the fluid flow and heat transfer close to the heater, so called near-field mechanisms. The literature investigating the near-field effects on CHF is summarized as follows:

Haramura and Katto [24] proposed a macrolayer dry-out model of CHF. The macrolayer is defined as a layer consisting of an array of small vapor jets underneath a large vapor mushroom. It was argued that CHF occurs when the liquid film in the macrolayer dries out before the mushroom departs. The obtained CHF model agrees well with Zuber's model (Eq. (2)).

Dhir and Liaw [9] presented a study investigating the contact angle effect on CHF. The void fraction in the macrolayer was measured experimentally to predict the CHF. Two conclusions were made: (i) CHF occur as a result of the hydrodynamic limit for fully wetting surfaces with contact angle smaller than 20°. (ii) For poorly wetting surfaces with contact angle larger than 20°, the CHF is due to the merging of small vapor stems in the macrolayer, given that higher CHF is observed for surfaces with smaller contact angles.

Kandlikar in 2002 [10] proposed a theoretical model accounting for wettability effects on CHF. His model is based on a force balance applied on a vapor bubble approaching CHF, which also shows a similar trend, i.e., CHF increases as contact angle reduces:

$$q_{CHF} = \rho_v h_{fg}\left(\frac{1+\cos\theta}{16}\right)\left[\frac{2}{\pi}+\frac{\pi}{4}(1+\cos\theta)\cos\Omega\right]^{1/2}\left[\frac{\sigma(\rho_l-\rho_v)g}{\rho_v^2}\right]^{1/4}. \tag{5}$$

The parameters θ and Ω are the contact angle and the angle relative to the horizontal, respectively.

Li and Peterson [18] used highly conductive microporous coated surfaces made of Cu wire meshes to increase the capillary force, which results in a higher CHF. Liter and Kaviany [19] also illustrated an enhancement of CHF on modulated porous layer coated surface as a result of a larger capillary limit. The capillary limit denotes the maximum flow rate that can be provided by the surface geometry. For a porous material, at CHF condition, the largest capillary pressure provided is balanced by a viscous pressure drag corresponding to the critical mass flow rate as shown:

$$\frac{\sigma}{r_c} = \frac{\mu\dot{m}_l\ell}{\rho_l\kappa A_c}, \tag{6}$$

where σ, r_c, μ, $\dot{m}_l$, l, ρ_l, κ, A_c are surface tension of liquid, minimum radius of curvature, liquid dynamic viscosity, liquid mass flow rate, liquid flow distance, liquid density, permeability and flowing

cross-sectional area, respectively. The minimum radius of curvature is equal to one-half of the interval between the characteristic features. The resultant CHF is equal to the product of the obtained maximum mass flow rate and the latent heat ($q_{CHF} = \dot{m}_l h_{fg}$).

Theofanous et al. [20] conducted a study investigating the phenomena of boiling crisis. They concluded that the boiling heat transfer is not dependent on the hydrodynamics but rather on the surface condition. Meanwhile, the CHF was found to have a direct correlation with the nucleation site density.

Honda and co-works [21–23] had shown that using micro pin–fins to enhance the CHF. The enhancement is attributed to an increase of nucleation site density and an increase of heat transfer surface area by the thermal fin effect.

1.3. Heater size effect

The effects of heater size on pool boiling have also been studied. Park and Bergles [25] conducted pool boiling of vertical heaters with one side insulated. The height and width of the heaters were systematically varied. It was shown that an increase of CHF was obtained as width decreased for heaters with small heights. Bar-Cohen and McNeil [26] determined the transitional point where heater size starts affecting CHF. The CHF becomes a function of the non-dimensional heater size $L'(= L/L_c)$ for $L' < 20$, where L is the heater length and L_c is the capillary length ($L_c = \sqrt{\sigma/[g(\rho_l - \rho_v)]}$). They attributed the effect of heater size on CHF to the transient conduction ability of the heater. On the other hand, Gogonin and Kutateladze [8] have shown that the heater size effect on CHF is absent for $L' > 2$ through a systematic experimental study. Lienhard and Dhir [2] argued that the variation of heater size can affect the CHF via reducing the number of vapor columns present on the heater surface. As the number of vapor columns is confined by the size of the heater, the area ratio (A_v/A_s) in Eq. (1a) is modified. Through a systematic study, it was shown that as the heater size is reduced to be smaller than three times the most dangerous Taylor instability wavelength ($L < 3 \times \lambda_D$ (i.e., $L' < 32$)) the CHF is a function of heater size [2]:

$$q_{CHF} = 1.14 \times q_{CHF,Z} \times \left(\frac{N_j \times \lambda_D^2}{A_s}\right), \tag{7}$$

where $q_{CHF,Z}$ is the CHF obtained from Eq. (2) and N_j is the number of vapor columns present on the surface. It is noted that this equation applies only for certain conditions where heater size is larger than the most dangerous wavelength ($L > \lambda_D$). Rainey and You [27] argued that for smaller heaters a significant portion of the heater is rewetted from the edges of the heater, which has a smaller flow resistance compared with larger heaters, resulting in a higher CHF. Kwark et al. [28] found a much stronger enhancement of CHFs on small heaters of boiling on nanofluid as compared to boiling on plain surfaces. They attributed the stronger heater size dependent on nanofluid is due to a better rewetting for the nanofluid-coated surfaces.

1.4. Boiling on nanostructured surfaces

Recent studies found boiling augmentation on nanostructured surfaces, such as nanofluids [11–17,28], Cu nanorods [29], carbon nanotubes (CNTs) [30,31], nano-fins [32], flower-like nanostructures [33], and nanowires [34]. The enhancement of CHF using nanofluids is mainly because of a change of surface property due to nanoparticle deposition. Here, a higher CHF is obtained for surfaces with smaller contact angles [11–15]. Meanwhile, for fully wetting surfaces with a zero contact angle, Kim et al. [11] have shown that a greater CHF is achieved for a surface with a larger capillary height where the height refers to the liquid column that can be sustained against gravity. This suggests that capillary force plays an important role in enhancing CHF. Ahn et al. [17] investigated the effect of liquid spreading on CHF using artificial surfaces with micro/nanostructures deposition similar to nano particles deposition. They attributed the enhancement of CHF to the increase of wettability and spreading ability on the artificial micro/nano structures.

In addition, Li et al. [29] reported a 200% increase in HTC due to the increase of nucleation site density using Cu nanorods. Ujereh et al. [30] reported the CHF augmentation by 45% on a CNT array due to the alternation of vapor embryo entrapment in the array and an increased surface area. Sathyamurthi et al. [31] also observed enhanced CHF by 58% on a CNT array due to an enhanced liquid–solid contact as a result of the disruption of microlayer by the CNT array. Sriraman [32] used nano-finned surfaces to enhance boiling heat transfer. He found that the CHF increases by 120% due to the presence of the nano-fins. Hendrick et al. [33] found an increase of CHF for saturated water on a flower-like nanostructures on Al surface of $\sim$82.5 W/cm^2 as compared to the CHF on a bare Al surface of $\sim$23 W/cm^2. They concluded that there is an optimized contact angle leading to a maximum CHF due to a balance between capillary force and bubble dynamics. Recently, we have reported a twofold enhancement in CHF on Cu and Si nanowire arrays [34] presumably because of a large capillary force provided by the nanowire arrays.

In summary, the mechanisms causing CHF can be broadly classified as far-field hydrodynamic instability-limited, e.g., Zuber [1] and Lienhard and Dhir [2] column Helmholtz–Taylor instability or near-field surface property-limited, e.g., the Katto vapor stem instability [24], wettability [9–16] and spreading ability [17], surface capillarity [18,19] and nucleation site density/bubble-dynamics instability [20–23,33]. Although much effort has been carried out to understand the mechanism of CHF for several decades, it is still an open question with regards to the exact mechanism causing CHF. General observations are that both the pool hydrodynamics and surface properties could affect the values of the CHF. In addition, it is agreed that the effect of heater size on CHF is to increase the value of the CHF. But the exact transition value of the size of the heater at which heater size starts to appear is not consistent [2,8,26]. Moreover, the underlying physics of the heater size effect on the CHF is not consistent either [2,26–28]. Motivated by these intriguing questions of boiling and CHF enhancements on nanofluids [11–17] and nanostructured surfaces [29–33], we seek to explore the mechanisms causing CHF on surfaces with high CHFs, e.g., surfaces coated with silicon nanowires [34]. As compared to boiling on the surfaces with random deposited nanoparticles [11–17], or on the nano-scale structures-patterned surfaces [29,32,33], or on the CNT arrays surfaces (which are hydrophobic) [30,31], the silicon nanowires coated-surfaces have the following advantages: (1) the surfaces have a well-controlled surface morphology; (2) the silicon nanowires are hydrophilic; (3) the length of the nanowire array can be easily controlled to tens to hundreds micrometers. Thus, it is believed that using the nanowires could enhance the performance of boiling and assist in exploring the mechanism of CHF. Previously we have shown that a surface coated with a vertical array of nanowires displays a much higher CHF and HTC as compared to a plain surface [34], which is consistent with our assumption and similar to the findings of boiling enhancement on nanostructured surfaces [29–33]. However, the exact mechanism causing CHF on these nanostructured surfaces is still unexplored. In this study, we seek to systematically examine the CHF mechanism on the nanowire array-coated surface by tailoring the length of the nanowires and the size of the heaters.

2. Nanowire synthesis

The SiNW coated-surface is obtained by wafer-scale electroless etching [35]. Briefly, the Si wafer is immersed in a 0.2 M HF

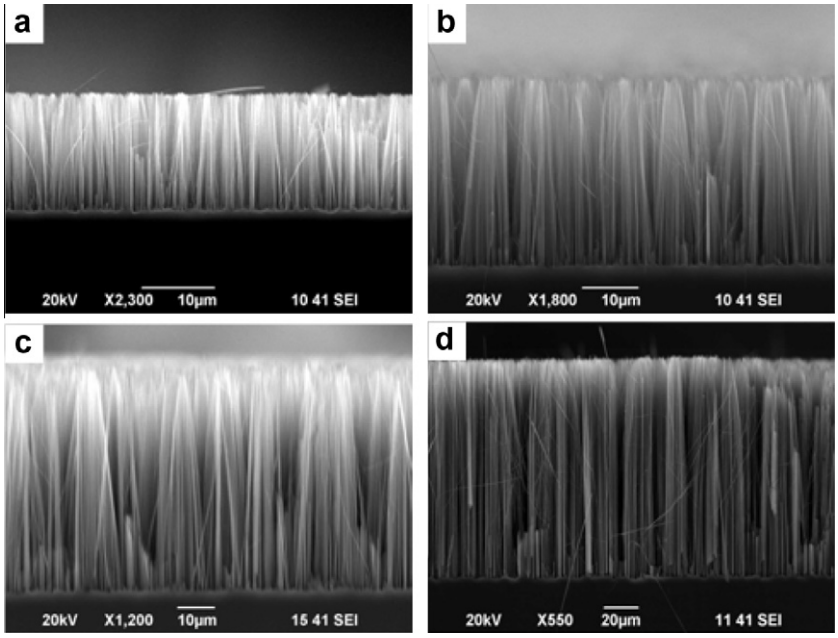

Fig. 1. SEM images of SiNW array with different heights: (a) ~16 μm, (b) ~32 μm, (c) ~59 μm, (d) ~122 μm.

solution with $AgNO_3$. A redox reaction occurs at the surface, oxidizing the area of Si surface not covered by deposited Ag particles. The oxidized area is then etched via HF solution successively forming an array of SiNWs. The height and density of the NW array are determined by the concentration and etching time; approximately ~50 μm height of SiNW array can be obtained after 2 h of etching. The obtained NWs have a diameter in a range between 50 and 300 nm (see Fig. 1).

3. Experimental setup and test section

The experimental setup and procedure conducted here are the same as that in our previous paper [34]. The test assembly was immersed in a pool of saturated de-ionized (DI) water throughout the experiment. The liquid temperature was kept at 100 °C for at least 30 min before power was applied to degas the water. The power was then supplied by a power supply (Agilent N5750A) to the indium-tin-oxide (ITO) heater. The wall temperature was measured by two thermocouples (T type, OMEGA Engineering Inc) directly soldered onto the ITO heater surface using thermal epoxy (EPOTEK 930, Epoxy Technology). The values of the temperature were recorded through the data acquisition system (Agilent 34970A). The CHF was postulated to be equal to the heating power corresponding to the last observed stable temperature, beyond which a sudden dramatic jump in heater temperature was observed.

The test sample including a Si substrate with nanowires and a heater was mounted to a Teflon block (thermal conductivity 0.2 W/m-K) to ensure thermal insulation (see supporting information in [34]). The test section is modified to reduce thermal spreading, i.e., lateral heat conduction within the wafer leading to an area of boiling larger than the heater. The reduction of thermal spreading is accomplished by a precisely defined heater area via backside lithography and a coating of low-conductivity photoresist (SU8, ~50 μm) over all areas not covered by the heater on the surface. The area covered by SiNWs is thus precisely aligned to the area on the wafer backside where the thin film heater of ITO is deposited. The resulting difference in thermal resistance and surface morphology between areas covered by the SU8 and the area covered by the SiNW array reduces bubbling at the edge of the heaters and a more accurate CHF based on the area of the heater can be obtained. The schematic of the test section is shown in Fig. 2.

In addition to the edge effect mentioned above, heat can still conduct through the Si substrate and this conduction heat loss is quantified as:

$$q_s = kA_c \frac{T_{edge} - T_{ref}}{d}, \tag{8}$$

where k, T_{edge}, T_{ref}, are thermal conductivity of Si substrate, temperature at the edge of the heater and temperature at distance of d away from the edge (see Fig. 2), respectively, whereas A_c is the cross-sectional area of heater which equals to the perimeter of the heater times the thickness of the wafer (~ 500 μm) and d is taken to be 2 mm.

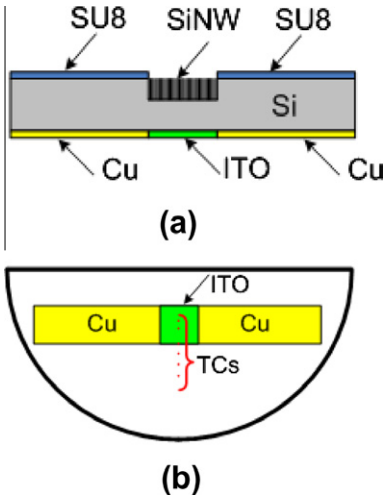

Fig. 2. Test section: (a) side view, (b) bottom view. A test section is designed to minimize thermal spreading via coating a layer of low-conductivity photoresist (SU8, ~50 μm) over all areas not covered by the heater on the surface and precisely aligning the area covered by SiNWs to the ITO heater area on the wafer backside.

4. Uncertainty analysis

The uncertainty of the measured heat fluxes is mainly from the accuracy of the power supply. The resultant relative uncertainty of the applied heat flux from the power supply (Agilent N5750A) is about 2%. The uncertainty of wall temperatures is from the estimated thickness of the epoxy layer ($k \sim 2$ W/m-K) and the resolution of the thermocouples. Assuming an uncertainty of the thickness of the epoxy layer of 5 μm, the uncertainty of the wall temperature due to the estimated thickness of the epoxy layer under 224 W/cm^2 (as in the case of CHF for a heater size of 0.5×0.5 cm^2 and assuming a 1.5% of the applied power is lost through the back side of the test section) is equal to 0.084 °C. The uncertainty of the absolute temperature measurement of the thermocouple is 0.5 °C and the accuracy of the thermocouple reading of the data acquisition system (Agilent 34970A) is 1 °C. Therefore, the overall uncertainty of the wall temperature measurement is about 1.584 °C. In addition, the uncertainty of the derived HTC is from the uncertainties of the applied heat flux and measured wall temperature. The resultant relative uncertainties of the HTCs are also about 2%. The above-mentioned uncertainties are attributed to as the systematic uncertainties. In addition, there are standard deviations of the multiple data points from various samples of the same morphology. The average values of the relative standard deviations of the CHFs on SiNW array-coated surfaces and plain Si surfaces are 6.5% and 16.4%, respectively. The standard deviations of the multiple data points of the CHF and HTC are large compared with the systematic uncertainties. The error bars and data range shown in the section of the results and discussion only include the standard deviations of multiple data points.

5. Results and discussion

5.1. Nanowire height effect on CHF

Both hydrodynamic instability and surface limited mechanisms leading to CHF are examined. First, the surfaces coated with SiNWs are superhydrophilic (zero contact angle (Fig. 3(b)) as compared to 40° on the plain Si surface (Fig. 3(a))), suggesting that wettability is not a limiting factor of CHF on the SiNW array-coated surfaces.

Pool boiling on the SiNW array-coated surfaces with four different NW lengths (~16, ~32, ~59 and ~122 μm as shown in SEM images of Fig. 1) with a heater area of 1 cm^2 has been carried out to investigate the capillary limit. The boiling curves are shown in Fig. 4(a) and (b). Fig. 4(a) compares our experimental results on the nanowire array-coated surface with the theoretical prediction of Rohsenow's correlation [36] and Fig. 4(b) shows our boiling results on the nanowire array-coated surfaces, a control experiment of boiling on a plain Si surface and the experimental results of boiling of nanofluid [16] and boiling on the copper nono-rod deposited surface [29]. The values of CHF and heat transfer coefficient, HTC (defined as the CHF divided by the superheat) for NW lengths of ~16, ~32, ~59 and ~122 μm are 162, 156, 159 ± 12 and 164 W/cm^2, respectively, and 5.59, 4.43, 4.68 ± 0.23 and 4.77 W/cm^2 K, respectively. The CHF values for these four lengths of NW array display a similar value of ~159 ± 9.71 W/cm^2. The values of CHF and HTC on the plain Si surface are 79 ± 15.52 W/cm^2 and 2.93 ± 0.47 W/cm^2 K, respectively. It indicates the boiling enhancement on the SiNW array-coated surfaces as compared to the plain Si surface. The enlarged CHF on the NW surface is due to a better liquid spreading on such surfaces (see Fig. 3). This is similar to previous findings of boiling enhancement of boiling of nanofluids [11–17,28], boiling on nanowires, and boiling on microporous surfaces [18,19]. Besides, the similar values of CHF for different heights of nanowires also suggest that the values of the CHF are not affected by the height of the NWs (see Fig. 4(b)). The boiling curves for the NW lengths of ~32, ~59 and ~122 μm approximately follow the Rohsenow's correlation [36] with $C_{sf} = 0.02$. The boiling curve of the 16 μm height NW array shows a distinct characteristic as compared to other lengths of the nanowires (see Fig. 4(a)). This might be due to the following reason: The microscale cavity distribution formed on the NW-coated surface is a result of surface tension-driven sticking of nanowires that occurs when the nanowires are removed from the etching solution [34]. It is possible that this process is altered as the height of the nanowires changes, resulting in a distribution with greater numbers of large cavities for smaller nanowire heights. As a result, the boiling curve of the 16 μm height nanowire array displays a lower wall superheat under the same applied heat flux as compared to the taller nanowires. The boiling curve on the nano-rod array-coated surface [29] (with 500 nm high and 0.8×0.8 cm^2 size) displays a higher slope as compared to the boiling curves on the SiNW array-coated surfaces. The CHF of 172 W/cm^2 of the copper nano-rod array is close to that on the SiNW array-coated surfaces (~159 W/cm^2). On the other hand, the boiling curve of the nanofluid [16] (having a cylindrical heater with a diameter of 2 cm and a thickness of 7 mm) has a lower slope as compared to the curves of the SiNW arrays. The CHF of the nanofluid display a higher value of 226 W/cm^2 as compared to those on the nano-rod array-coated surface (172 W/cm^2) and SiNW array-coated surfaces (~159 W/cm^2).

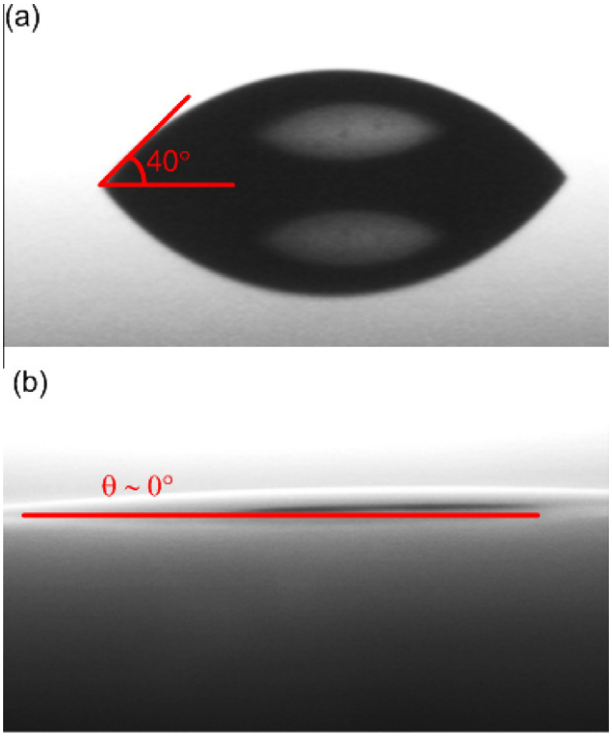

Fig. 3. Contact angle of water on: (a) plain Si surface with a contact angle of 40°, (b) SiNW array-coated surface with a zero contact angle.

The condition of the capillary limit is depicted by Eq. (6) at which the maximum flow rate is obtained corresponding to a minimum radius of curvature (r_c). Since these nanowire arrays create the dominant flow resistance in the system, the maximum flow rate (the capillary limit) should be inversely proportional to the length of the nanowire provided that the maximum capillary pressure (σ/r_c) is the same for the different heights of nanowires. The fact that the CHFs are independent of nanowire heights suggests that the CHFs of the NW array-coated surfaces are not due to the capillary limit. Meanwhile, the obtained CHF of ~159 ± 9.71 W/cm^2 is superior to ~110 W/cm^2 or 126 W/cm^2 as predicted by

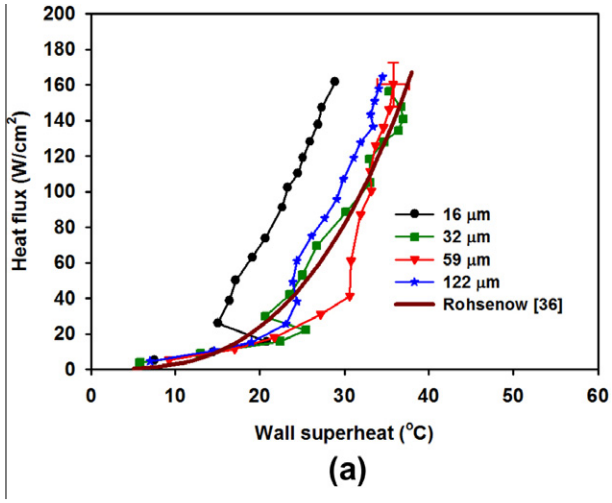

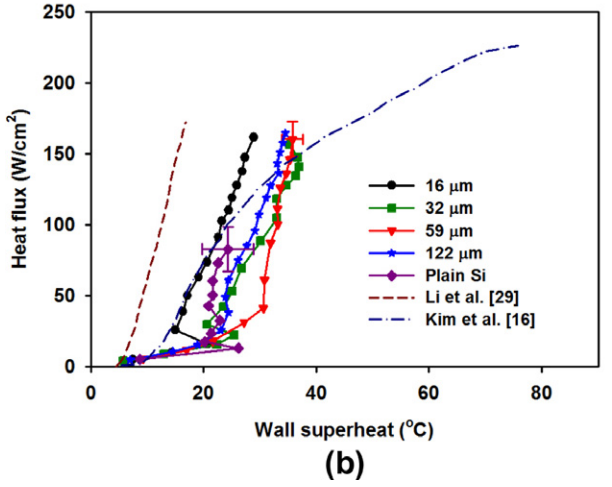

Fig. 4. (a) Boiling curves on SiNW array-coated surfaces for different heights of NWs compared with Rohsenow's correlation [36]. (b) Boiling curves on the SiNW arrays, on the plain Si surface, and the experimental results of boiling of nanofluid [16] and boiling on nano-rod array-coated surface [29]. It indicates that the values of CHFs are not affected by the height of the nanowires.

the hydrodynamic limits of saturated water (Eqs. (2) and (3)), which seems to suggest that the hydrodynamic limit does not apply to the surfaces as well. However, it is noted that the model is applied to an infinite heater surface in which the Helmholtz wavelength was assumed to be equal to the most dangerous Taylor wavelength ($\lambda_H = \lambda_D$) and the diameter of the vapor column and the spacing of vapor columns are $\lambda_D/2$ and λ_D, respectively, resulting in an area ratio of vapor columns and heater surface (A_v/A_s in Eq. (1a)) of $\pi/16$. This Taylor wavelength (λ_D) for saturated water (2.5 cm) is larger than the heater size adopted of 1 cm^2 given that only one vapor column can be present on the heater surface. Thus, the small size of heater may limit the value of the Helmholtz wavelength resulting in a heater size effect on CHF.

5.2. Heater size effect on CHF

To address this, pool boiling experiments on SiNW array-coated surfaces with various heater sizes have been carried out. The boiling curves of ~50 μm height SiNW array-coated surfaces with four different sizes of heaters are shown in Fig. 5. Images of bubbles at these heaters at CHF condition are shown in Fig. 6. Note that only one vapor column/mushroom is present for all the sizes of the heaters at CHF condition. The CHFs and HTCs for heater sizes of 0.5×0.5, 1×1, 1.5×1.5 and 2×2 cm^2 after subtracting heat

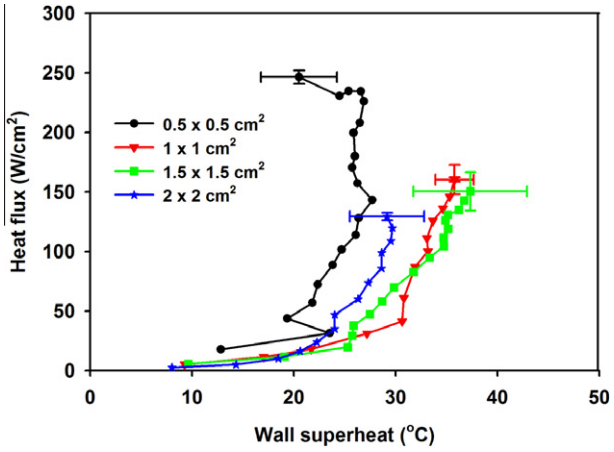

Fig. 5. Boiling curves on SiNW array coated surfaces for different sizes of the heaters, which indicates that CHF increases as heater size reduces.

conduction losses (Eq. (8)) are shown in Table 1. The CHF increases as heater size reduces. The obtained highest CHF and HTC of 223.90 ± 5.61 W/cm^2 and 9.06 ± 1.60 W/cm^2 K, respectively, on a heater size of 0.5×0.5 cm^2 are among the peak values reported in boiling heat transfer. The corresponded percentage of the heat conduction losses of the CHFs for various sizes of the heaters are also shown in Table. 1. The conduction losses for various sizes of heaters are about $6.26 \pm 1.60\%$ of the CHF.

There are at least four different models of CHF: (1) the Zuber [1] and Lienhard and Dhir [2] column Helmholtz–Taylor instability model, (2) the Katto vapor stem instability [24], (3) wettability [9–16], spreading ability [17] and surface capillarity [18,19] and (4) nucleation site density/bubble-dynamics instability [20–23,33].

Since there is only one vapor column presented on the small size heaters, the observed heater size dependence of CHFs cannot be explained by the model of Eq. (7) proposed by Lienhard and Dhir [2] which assumes that the effect of heater size is due to a reduction of the number of vapor columns. Furthermore, the results of CHFs for different heights of nanowires indicate that the capillarity or spreading ability on such surfaces are not the limiting force for CHFs (as already discussed in Section 5.1). Moreover, the heater size dependent CHF cannot be explained by the models of nucleation site density/bubble-dynamics instability [20–23,33] since the nucleation site density/bubble dynamics should not be a function of heater size. Thus, the hydrodynamic instability is most likely responsible for the CHFs on the nanowire array-coated surfaces. Assuming the hydrodynamic instability is the mechanism causing CHFs, we need to know the Helmholtz wavelength and the area ratio (λ_H and A_v/A_s, respectively, in Eq. (1a)) to correctly calculate the values of CHFs on these small size heaters. The original Helmholtz wavelength in the hydrodynamic theory is assumed equal to the most dangerous Taylor wavelength ($\lambda_H = \lambda_D = 2.5$ cm), which is bigger than the heater size studied here. Thus, we believed that it is not appropriated to assume the same value to the Helmholtz wavelengths on the small heaters studied here. We speculate that the actual Helmholtz wavelength might be affected by the size of the heater and it is adopted as a control variable for the theoretical study of the hydrodynamic theory. Furthermore, the area ratio of $\pi/16$ in the models of Zuber [1], Lienhard and Dhir [2] is obtained from the ratio of the area covered by the vapor columns and the heater ($[(\pi/4)\cdot(\lambda_D/2)^2]/\lambda_D^2 = \pi/16$). But in the present study, there is only one vapor column presented on the small heaters. Thus, the area ratio might not be the same as that in the hydrodynamic models [1,2]. The area ratio for a heater having only one vapor column/mushroom should be proportional to the number of vapor stems in the macrolayer. The number of

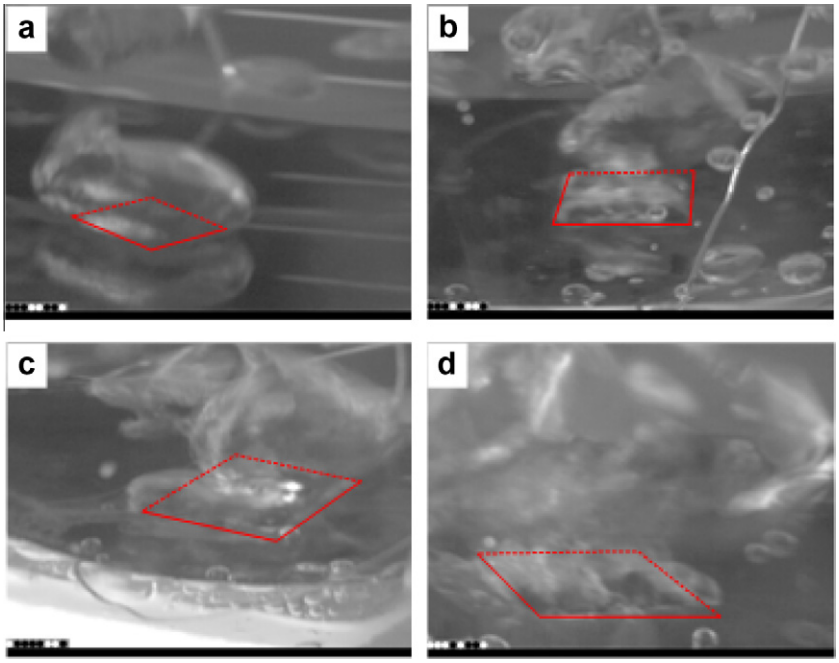

Fig. 6. Boiling images at CHF condition for different sizes of heaters: (a) 0.5 × 0.5 cm^2, (b) 1 × 1 cm^2, (c) 1.5 × 1.5 cm^2 and (d) 2 × 2 cm^2. Only one vapor column/mushroom is present for all the sizes of the heaters, note that the edges of heaters are outlined.

Table 1
Summary of experimental results.

		Heater size			
		0.5 × 0.5 (cm^2)	1 × 1 (cm^2)	1.5 × 1.5 (cm^2)	2 × 2 (cm^2)
SiNW	CHF (W/cm^2)	223.90 ± 5.61	150.67 ± 12.42	124.85 ± 16.21	125.52 ± 3.06
	HTC (W/cm^2 K)	9.06 ± 1.60	4.68 ± 0.23	3.89 ± 0.64	4.84 ± 0.72
	Conduction loss (%)	7.03	7.96	5.80	4.26
Plain Si	CHF (W/cm^2)	81.48 ± 0.87	67.40 ± 15.52	46.82 ± 6.46	44.22 ± 12.33
	HTC (W/cm^2 K)	2.98 ± 1.01	2.80 ± 0.47	1.82 ± 0.29	1.93 ± 0.73
	Conduction loss (%)	16.21	13.46	17.88	10.08

vapor stem is directly related to the nucleation site density on the surfaces and has been demonstrated by Dhir and Liaw [9] as a function of the contact angle on the surface. However, we were unable to directly measure the area ratio on the heater surface in the current experimental setup. Thus, the area ratio in Eq. (1a) is adopted as a fitting factor here for the modeling of the hydrodynamic theory.

Therefore, we use the modified hydrodynamic model (Eq. (1a)) to calculate the CHF on various heater sizes, in which λ_H is a control variable and A_v/A_s is a fitting factor for perdition.

The measured CHFs (after subtracting heat conduction losses in Si substrate) versus heater size along with the theoretical prediction of the modified hydrodynamic theory are shown in Fig. 7. The red filled circle marks are experimental results of SiNW array-coated surfaces of four different sizes of heaters. The red solid curve is the theoretical prediction of Eq. (1a) using the Helmholtz wavelength as a control variable assuming an area ratio (A_v/A_s) of 0.15. It can be seen that the experimental results can qualitatively match the theory via assuming the Helmholtz wavelength equal to the corresponded heater size. It is, therefore, postulated that for heaters with only one vapor column presents on the surface, the size of the heater poses a critical wavelength resulting in the instability of vapor columns.

As a control experiment, the boiling curves for plain Si surfaces with corresponded heater sizes are shown in Fig. 8. The CHFs and

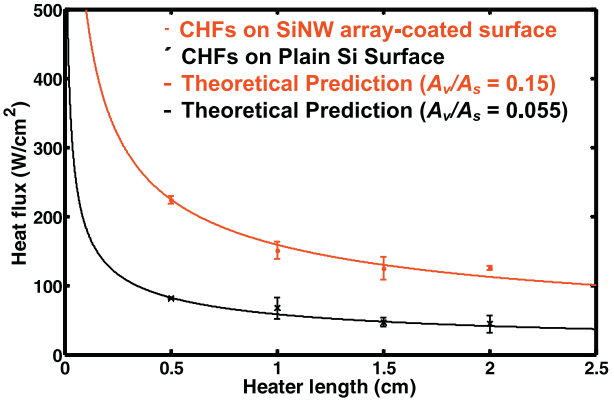

Fig. 7. CHF versus heater length (after subtracting conduction loss in Si substrate) where the red filled circle marks are experiment results of SiNW array-coated surfaces of four different sizes of heaters and the red solid curve is the theoretical prediction of hydrodynamic theory using the Helmholtz wavelength as a control variable assuming an area ratio (A_v/A_s) of 0.15 and the dark cross points are the results of plain Si surfaces and the dark solid curve is the theoretical prediction of hydrodynamic theory assuming an area ratio (A_v/A_s) of 0.055.

HTCs for the heater sizes after subtracting heat conduction losses (Eq. (8)) are shown in Table 1. The obtained highest CHF and HTC

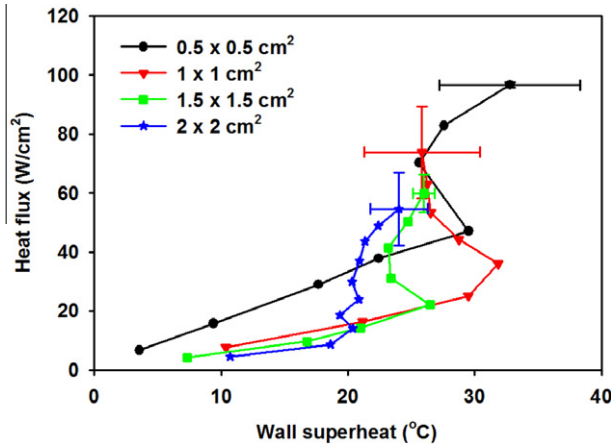

Fig. 8. Boiling curves on plain Si surfaces for different sizes of heaters, which shows that CHF increases as heater size reduces.

are 81.48 ± 0.87 W/cm^2 and 2.98 ± 1.01 W/cm^2 K, respectively, on a heater size of 0.5 × 0.5 cm^2. The percentages of the heat conduction losses of the CHFs are also shown in Table 1. The conduction losses for various sizes of heaters are about 14.40 ± 3.41% of the CHF. Since the HTCs on the plain Si surfaces are smaller than that on the nanowire array-coated surfaces, the correspondingly higher conduction losses are observed on the plain Si surfaces. These values of CHFs along with the theoretical prediction using modified hydrodynamic model (Eq. (1a)) having an area ratio (A_v/A_s) of 0.055 for plain Si surfaces are also shown in Fig. 7 (dark cross points and dark solid curve, respectively). The CHFs on the plain Si surface could also be matched by the hydrodynamic theory by assuming the Helmholtz wavelength equal to the heater length with a smaller area ratio of 0.055 as compared to the nanowire array-coated surfaces (see Fig. 7). The use of a higher area ratio for the nanowire array-coated surface is supported by the fact that a larger nucleation site density is observed on the nanowire array-coated surfaces as compared to the plain Si surfaces.

6. Conclusion

The experimental results indicate that both the liquid spreading and the size of heater can retard the occurrence of CHF. The enhancement of CHF on SiNW array coated surface as compared to the plain Si surface is because of a better liquid spreading on the NW array surface. Meanwhile, the increase of CHF as heater size reduces is an indication of heater size effect on CHF. The heater size effect appears when the heater length is approximately smaller than 8 times the capillary length (i.e., $L' < 8$). The CHFs on SiNW and plain Si surfaces for different sizes of heaters clearly indicate that the two effects (liquid spreading and heater size) on CHF are simultaneous and additive. In addition, the agreement of experimental results with theoretical predication of the hydrodynamic theory may suggest that the effect of heater size is due to a confined Helmholtz wavelength by the small-sized heaters. Meanwhile, both the CHFs on SiNW array-coated and plain Si surfaces might be limited by pool hydrodynamics.

Acknowledgments

This work was supported by Intel Corporation and the UC Discovery program. We thank the UC Berkeley Micro-fabrication Laboratory for the use of their facilities. The authors thank Dr. R.S. Prasher of Advanced Research Projects Agency-Energy and Dr. J.-Y. Chang of Intel for helpful discussions on boiling heat transfer.

References

[1] N. Zuber, Hydrodynamic Aspects of Boiling Heat Transfer, AECU-4439, 1959.
[2] J.H. Lienhard, V.K. Dhir, Hydrodynamic Theory of the Peak and Minimum Pool Boiling Heat Fluxes, CR-2270, 1973.
[3] V.P. Carey, Liquid–Vapor Phase-Change Phenomena: An Introduction to the Thermophysics of Vaporization and Condensation Processes in Heat Transfer Equipment, second ed., Taylor and Francis, New York, 2008.
[4] G. Birkhoff, Helmholtz and Taylor instability, Proceedings of Symposia in Applied Mathematics, vol. 13, American Mathematical Society, Providence, Rhode Island, 1962, pp. 55–76.
[5] J.W.S. Rayleigh, On the instability of jets, in: Proceedings of the London Mathematical Society, vols. s1–10, 1879, pp. 4–13, Available from: <http://plms.oxfordjournals.org/content/s1-10/1/4.extract>.
[6] D.H. Sharp, An overview of Rayleigh–Taylor instability, Physica D 12 (1984) 3–10.
[7] S.S. Kutateladze, A hydrodynamic theory of changes in a boiling process under free convection, in: Izvestia Akademia Nauk, S.S.S.R., Otdelenie Tekhnicheski Nauk, vol. 4, 1951, p. 529.
[8] I.I. Gogonin, S.S. Kutateladze, Critical heat flux as a function of heater size for a liquid boiling in a large enclosure, J. Eng. Phys. 33 (1977) 1286–1289.
[9] V.K. Dhir, S.P. Liaw, Framework for a unified model for nucleate and transition pool boiling, J. Heat Transfer 111 (1989) 739–745.
[10] S.G. Kandlikar, A theoretical model to predict pool boiling CHF incorporating effects of contact angle and orientation, J. Heat Transfer 123 (6) (2001) 1071–1079.
[11] H.D. Kim, M.H. Kim, Effect of nanoparticle deposition on capillary wicking that influences the critical heat flux in nanofluids, Appl. Phys. Lett. 91 (1) (2007) 0141040-1–0141040-3.
[12] S.J. Kim, I.C. Bang, J. Buongiomo, L.W. Hu, Study of pool boiling and critical heat flux enhancement in nanofluids, Bull. Polish Acad. Sci. Tech. Sci. 55 (2) (2007) 211–216.
[13] S.J. Kim, I.C. Bang, J. Buongiorno, L.W. Hu, Effects of nanoparticle deposition on surface wettability influencing boiling heat transfer in nanofluids, Appl. Phys. Lett. 89 (15) (2006) 153107-1–153107-3.
[14] S.J. Kim, I.C. Bang, J. Buongiorno, L.W. Hu, Surface wettability change during pool boiling of nanofluids and its effect on critical heat flux, Int. J. Heat Mass Transfer 50 (19-20) (2007) 4105–4116.
[15] S.M. You, J.H. Kim, K.H. Kim, Effect of nanoparticles on critical heat flux of water in pool boiling heat transfer, Appl. Phys. Lett. 83 (16) (2003) 3374–3376.
[16] H. Kim, H.S. Ahn, M.H. Kim, On the mechanism of pool boiling critical heat flux enhancement in nanofluids, J. Heat Transfer 132 (6) (2010) 0615011-1–0615011-11.
[17] H.S. Ahn, H.J. Jo, S.H. Kang, M.H. Kim, Effect of liquid spreading due to nano/microstructures on the critical heat flux during pool boiling, Appl. Phys. Lett. 98 (7) (2011) 071908-1–071908-3.
[18] C. Li, G.P. Peterson, Parametric study of pool boiling on horizontal highly conductive microporous coated surfaces, J. Heat Transfer 129 (11) (2007) 1465–1475.
[19] S.G. Liter, M. Kaviany, Pool-boiling CHF enhancement by modulated porous-layer coating: theory and experiment, Int. J. Heat Mass Transfer 44 (22) (2001) 4287–4311.
[20] T.G. Theofanous, T.N. Dinh, J.P. Tu, A.T. Dinh, The boiling crisis phenomenon – part II: dryout dynamics and burnout, Exp. Therm. Fluid Sci. 26 (6–7) (2002) 793–810.
[21] H. Honda, H. Takamastu, J.J. Wei, Enhanced boiling of FC-72 on silicon chips with micro-pin-fins and submicron-scale roughness, J. Heat Transfer 124 (2) (2002) 383–390.
[22] J.J. Wei, H. Honda, Effects of fin geometry on boiling heat transfer from silicon chips with micro-pin-fins immersed in FC-72, Int. J. Heat Mass Transfer 46 (21) (2003) 4059–4070.
[23] H. Honda, J.J. Wei, Enhanced boiling heat transfer from electronic components by use of surface microstructures, Exp. Therm. Fluid Sci. 28 (2–3) (2004) 159–169.
[24] Y. Haramura, Y. Katto, A new hydrodynamic model of critical heat-flux, applicable widely to both pool and forced-convection boiling on submerged bodies in saturated liquids, Int. J. Heat Mass Transfer 26 (3) (1983) 389–399.
[25] K.A. Park, A.E. Bergles, Effects of size of simulated microelectronic chips on boiling and critical heat-flux, J. Heat Transfer 110 (3) (1988) 728–734.
[26] A. Bar-Cohen, A. McNeil, Parametric effects of pool boiling critical heat flux in dielectric liquids, in: Proceedings of the Engineering Foundation Conference on Pool and External Flow Boiling, ASME, Santa Barbara, CA, 1992, pp. 171–175.
[27] K.N. Rainey, S.M. You, Effects of heater size and orientation on pool boiling heat transfer from microporous coated surfaces, Int. J. Heat Mass Transfer 44 (14) (2001) 2589–2599.
[28] S.M. Kwark, M. Amaya, R. Kumar, G. Moreno, S.M. You, Effects of pressure, orientation, and heater size on pool boiling of water with nanocoated heaters, Int. J. Heat Mass Transfer 53 (23–24) (2010) 5199–5208.
[29] C. Li, Z. Wang, P.I. Wang, Y. Peles, N. Koratkar, G.P. Peterson, Nanostructured copper interfaces for enhanced boiling, Small 4 (8) (2008) 1084–1088.
[30] S. Ujereh, T. Fisher, I. Mudawar, Effects of carbon nanotube arrays on nucleate pool boiling, Int. J. Heat Mass Transfer 50 (19–20) (2007) 4023–4038.

[31] V. Sathyamurthi, H.S. Ahn, D. Banerjee, S.C. Lau, Subcooled pool boiling experiments on horizontal heaters coated with carbon nanotubes, J. Heat Transfer 131 (7) (2009) 071501-1–071501-10.
[32] S.R. Sriraman, Pool Boiling on Nano-Finned Surfaces, Master Thesis, Texas A&M University, College Station, TX, 2007.
[33] T.J. Hendricks, S. Krishnan, C. Choi, C.-H. Chang, B. Paul, Enhancement of pool-boiling heat transfer using nanostructured surfaces on aluminum and copper, Int. J. Heat Mass Transfer 53 (15–16) (2010) 3357–3365.
[34] R. Chen, M.C. Lu, V. Srinivasan, Z. Wang, H.H. Cho, A. Majumdar, Nanowires for enhanced boiling heat transfer, Nano Lett. 9 (2) (2009) 548–553.
[35] A.I. Hochbaum, R.K. Chen, R.D. Delgado, W.J. Liang, E.C. Garnett, M. Najarian, A. Majumdar, P.D. Yang, Enhanced thermoelectric performance of rough silicon nanowires, Nature 451 (7175) (2008) 163–167.
[36] W.M. Rohsenow, A method of correlating heat transfer data for surface boiling of liquids, Trans. ASME 74 (1952) 969–975.